Rapid Communications

Interface-induced spin-orbit interaction in silicon quantum dots and prospects for scalability

Rifat Ferdous,[1,*] Kok W. Chan,[2,†] Menno Veldhorst,[3] J. C. C. Hwang,[2] C. H. Yang,[2] Harshad Sahasrabudhe,[1] Gerhard Klimeck,[1] Andrea Morello,[2] Andrew S. Dzurak,[2] and Rajib Rahman[1]

[1]*Network for Computational Nanotechnology, Electrical and Computer Engineering, Purdue University, West Lafayette, Indiana 47907, USA*

[2]*Centre for Quantum Computation and Communication Technology, School of Electrical Engineering and Telecommunications, The University of New South Wales, Sydney, New South Wales 2052, Australia*

[3]*QuTech and Kavli Institute of Nanoscience, TU Delft, Lorentzweg 1, 2628 CJ Delft, The Netherlands*

(Received 3 May 2017; revised manuscript received 11 May 2018; published 4 June 2018)

We identify the presence of monatomic steps at the Si/SiGe or Si/SiO_2 interface as a dominant source of variations in the dephasing time of silicon (Si) quantum dot (QD) spin qubits. First, using atomistic tight-binding calculations we show that the g-factors and their Stark shifts undergo variations due to these steps. We compare our theoretical predictions with experiments on QDs at a Si/SiO_2 interface, in which we observe significant differences in Stark shifts between QDs in two different samples. We also experimentally observe variations in the g-factors of one-electron and three-electron spin qubits realized in three neighboring QDs on the same sample, at a level consistent with our calculations. The dephasing times of these qubits also vary, most likely due to their varying sensitivity to charge noise, resulting from different interface conditions. More importantly, from our calculations we show that by employing the anisotropic nature of the spin-orbit interaction (SOI) in a Si QD, we can minimize and control these variations. Ultimately, we predict that the dephasing times of the Si QD spin qubits will be anisotropic and can be improved by at least an order of magnitude, by aligning the external dc magnetic field towards specific crystal directions, given other decoherence mechanisms do not dominate over charge noise.

DOI: 10.1103/PhysRevB.97.241401

A scalable quantum computing architecture requires reproducibility and control over key qubit properties, such as resonance frequency, coherence time, etc. Variability in such parameters among qubits of a large-scale quantum computer would necessitate individual qubit characterization and control [1], while excessive variability could even make scaling impractical. In case of significant variability in the dephasing time, the qubit that decoheres the fastest might limit the overall performance.

Spin qubits hosted in Si quantum dots (QDs) [2] have been showing promise as a potential building block for a large-scale quantum computer [3], because of their compatibility with already existing complementary metal-oxide-semiconductor (CMOS) technology and the long coherence times available due to the presence of negligible nuclear spins in isotopically purified ^{28}Si [4]. Single- [5–10] and two-qubit [11] gates have been demonstrated already. To move forward with increasing numbers of qubits [1,12–14], we have to study the possible sources that can cause variations in the coherence time and limit the performance of these qubits.

In this Rapid Communication, we provide a microscopic understanding of the dephasing time T_2^* of Si QD spin qubits. We show that electrical noise modulates the electron g-factor through a spin-orbit interaction (SOI) and causes dephasing. Moreover, the atomic-scale details of the interface control the sensitivity of the g-factor to the electric field or noise and hence introduce variability in the T_2^* times. We experimentally observe variations in the g-factors, their gate voltage dependence, and T_2^* times among spin qubits hosted in gate-defined quantum dots formed at a Si/SiO_2 interface. Finally, we predict that, due to the anisotropic nature of the SOI in Si QDs, the T_2^* times will be anisotropic and hence can be improved and their variability can be reduced as well by choosing the appropriate direction of the external magnetic field.

The energy levels of interest in a Si QD for qubit operations are two low-lying conduction band valley states v_- and v_+, each split in two spin levels in the presence of a dc magnetic field B_{ext}. All subsequent symbols with a subscript $-$ $(+)$ correspond to the v_- (v_+) valley state. However, it turns out that the spin splitting ($E_{ZS}^{\pm} = g_{\pm}\mu_B B_{\text{ext}}$, where μ_B is the Bohr magneton) and also the dephasing time T_2^* are valley dependent [9,15–18] and, as we will show experimentally, is sample-to-sample dependent.

In a Si quantum well or dot, the presence of structure inversion asymmetry introduces the Rashba SOI [19–21]. Though it is known that due to the lack of bulk inversion asymmetry, the Dresselhaus SOI is absent from bulk Si, interface inversion asymmetry contributes a Dresselhaus-like term in interface-confined structures in Si [19–21]. Both the Rashba and Dresselhaus SOI modify the electron g-factors in a Si QD, and enable the Stark shift of the g-factors through gate voltage tuning [8,15,22]. The different sign of the Rashba ($\alpha_{\pm}$) and Dresselhaus coefficients ($\beta_{\pm}$) results in different g-factors among the two valley states [15]. The Dresselhaus contribution is usually much stronger than the Rashba SOI [18,21], and dominates the g-factor renormalization [18].

*rferdous@purdue.edu
†kokwai@unsw.edu.au

These SOI effects also make the qubits susceptible to electrical noise.

In a Si QD with a strong vertical electric field, the electrons are usually confined to only one interface. A monatomic shift in the location of this interface results in a sign inversion of the Dresselhaus coefficient, while the Rashba coefficient remains unchanged [19–21]. In practice, Si/SiGe or Si/SiO_2 interfaces certainly contain roughness, i.e., monatomic steps [23–25]. A nonideal interface with monatomic steps can be thought of as multiple smooth interface regions, where interfaces of neighboring regions are shifted by one atomic layer with respect to each other. Thus the neighboring regions will have opposite signs of β. An electron wave function spread over multiple such regions will witness multiple local β's and the effective β will be a weighted average. Thus the presence of interface steps can change both the sign and magnitude of the effective Dresselhaus contribution to the electron g-factors in a Si QD [18]. In essence, local changes in the orientation of the chemical bonds of the atoms at the interface inside a dot may result in similar effects. To accurately understand these atomic-scale physics of the interface, here we use a spin-resolved $sp^3d^5s^*$ tight-binding model, where the effects of the SOI come out automatically based on the atomic arrangement of the QD, without any preassumption about the Rashba or Dresselhaus SOI.

Figure 1 shows how a monatomic step at the interface of a Si QD can affect the g-factors of the valley states and their electric field dependence, with an external magnetic field along the [110] crystal orientation, from atomistic tight-binding simulations. The distance between the dot center and the location of the edge of the interface step is denoted by x_0 [shown in Fig. 1(a)]. The dot radius is around 10 nm. So for $x_0 < -10$ nm the dot is completely on the left side of the step and has different g-factors ($g_- > g_+$) compared to that ($g_+ > g_-$) for $x_0 > 10$ nm, when the dot is completely on the right side of the step, as seen in Fig. 1(b). For -10 nm $< x_0 <$ 10 nm, the g-factors are a weighted average of those of the two sides based on the dot location. To understand this atomistic calculation we use an analytic effective mass model that relates $g_\pm$ in a Si QD, with the Rashba and Dresselhaus SOI [15,18]. We briefly summarize this model in the Supplemental Material [26]. For B_{ext} along the [110] crystal orientation,

$$\delta g_\pm^{[110]} = g_\pm^{[110]} - g_\perp = 2\frac{|e|\langle z\rangle}{\mu_B\hbar}(-\alpha_\pm + \beta_\pm). \qquad (1)$$

Here, $g_\perp = 1.9937$ is the g-factor perpendicular to the valley axis [18,27], $|e|$ is the electron charge, $\langle z\rangle$ is the spread of the electron wave function along the vertical direction z ([001]), and $\hbar$ is the reduced Planck constant. Now, in a Si QD, $\beta \gg \alpha$ [18,21], and so

$$\delta g_\pm^{[110]} \approx 2\frac{|e|\langle z\rangle}{\mu_B\hbar}\beta_\pm. \qquad (2)$$

As previously discussed, β has a different sign between the two sides of the step. When the location of the dot changes with respect to the step, the weighted average of the positive and negative β's changes, which changes the g-factors.

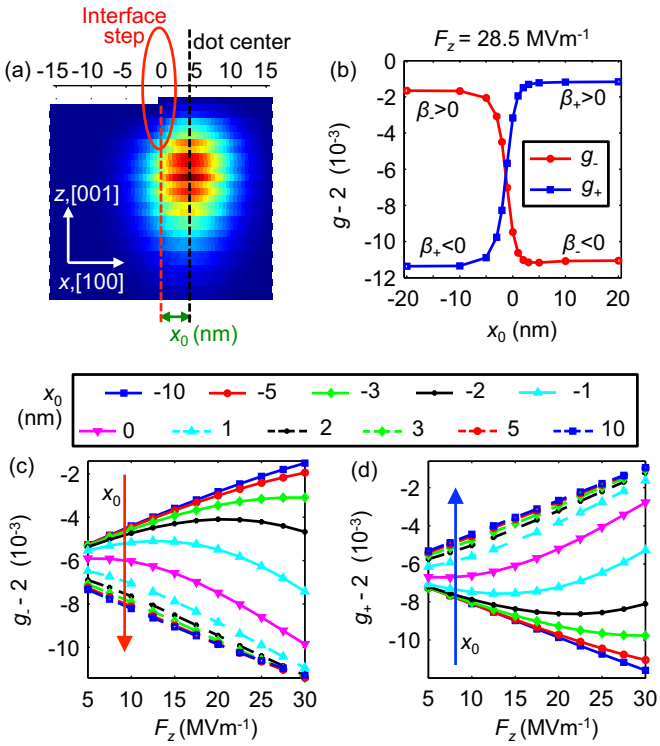

FIG. 1. Effect of interface steps on g-factors and their Stark shifts in a Si QD from an atomistic tight-binding calculation. (a) An electron wave function subject to an interface step. (b) Variation in the g-factors for both valley states (g_- and g_+), as a function of x_0 for a vertical electric field $F_z = 28.5$ MV m^{-1} [22]. When the electron is on the left (right) side of the step, β_- is positive (negative) and β_+ is negative (positive), and we see $g_- > g_+$ ($g_- < g_+$). F_z dependence of (c) g_- and (d) g_+ for various x_0. The magnetic field used in the simulations of (b)–(d) is 1.4 T along the [110] crystal orientation and the monatomic step is parallel to the y ([010]) direction.

Figures 1(c) and 1(d) show that the Stark shifts of the g-factors, as a function of the confining vertical electric field F_z, for both valley states are also affected by the presence of an interface step. The differential change in the g-factors with electric field, $\frac{dg_\pm}{dF_z}$, can vary in both sign and magnitude depending on the location of the step. This behavior can also be explained by Eq. (2), with the change in β near an interface step. For example, in Fig. 1(c), for $x_0 \approx -10$ nm, the dot is completely on the left side of the step, where the v_- valley state has positive β. Thus an increase in β_- with increasing F_z increases g_- as well, hence a positive $\frac{dg_-}{dF_z}$. On the other hand, when the dot is completely on the right side of the step, at $x_0 \approx 10$ nm, β_- is negative. Thus increasing F_z increases $|\beta_-|$ but decreases g_- and thus results in a negative $\frac{dg_-}{dF_z}$. For -10 nm $< x_0 < 10$ nm, $\frac{dg_-}{dF_z}$ changes gradually with x_0. We see a similar but opposite change for g_+ in Fig. 1(d).

Similar variations in the g-factors, and their gate voltage dependence, are measured in gate-defined quantum dots formed at a Si/SiO_2 interface for two different samples (A and B) with similar architecture. Figure 2(b) shows variations in one-electron and three-electron g-factors among Q_1, Q_2 and

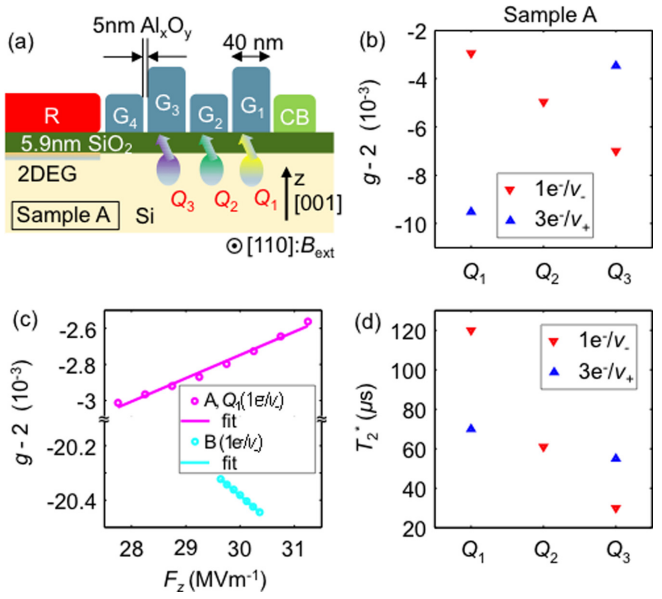

FIG. 2. Schematic diagram of the experimental sample and observed dot-to-dot variations. (a) Cross-sectional schematic of sample A. The confinement barrier gate (CB) acts as a lateral confinement gate in the formation of quantum dots under gates G_1, G_2, and G_3. G_4 is used as a tunnel barrier for loading/unloading of electrons from the 2DEG formed under the reservoir (R) gate. The external magnetic field is applied along the [110] crystal orientation, which is going out of the plane of the paper. (b) Variation in the g-factors, both one-electron (g_-) and three-electron (g_+), among three neighboring quantum dots (Q_1, Q_2, Q_3) formed at the Si/SiO_2 interface in sample A. (c) One-electron Stark shift of Q_1 from sample A and one QD from sample B plotted together as a function of the vertical electric field F_z. Note that both samples were measured in different dilution fridges and there is an unknown B_{ext} offset in sample B, contributing to a larger discrepancy in its g-factor from 2. (d) Observed variations in the dephasing times among qubits in sample A.

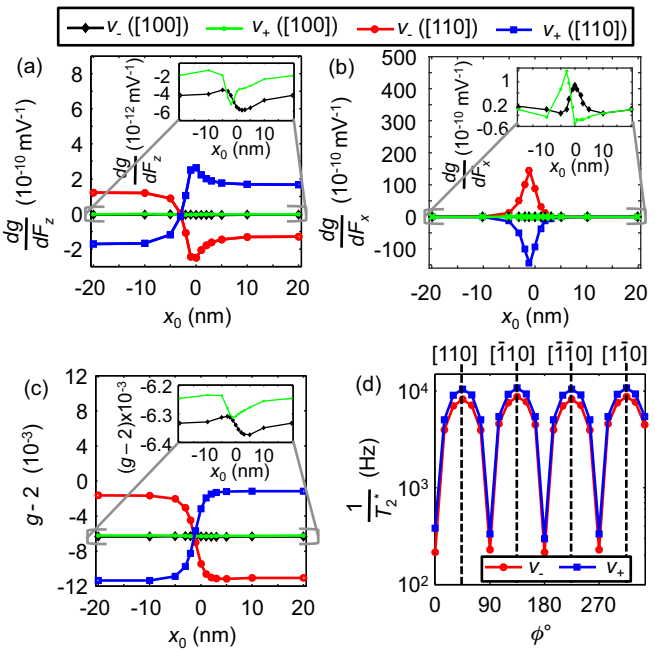

FIG. 3. Change in (a) $\frac{dg_\pm}{dF_z}$, (b) $\frac{dg_\pm}{dF_x}$, and (c) $g_\pm$ as a function of x_0 with B_{ext} along [110] and [100] (inset), for $F_z = 28.5$ MV m^{-1}, calculated using an atomistic tight-binding model. (d) $\frac{1}{T_2^*} = \frac{1}{T_2^*(\Delta F_z)} + \frac{1}{T_2^*(\Delta F_x)}$ with respect to the direction of B_{ext}, ϕ, for $x_0 = -6$ nm, $F_z = 28.5$ MV m^{-1}, and $B_{ext} = 1.4015$ T. T_2^* is calculated using Eq. (3) for $\Delta F_z = 400$ V m^{-1} and $\Delta F_x = 80$ V m^{-1}, with $\frac{dg_\pm}{dF_z}$ and $\frac{dg_\pm}{dF_x}$ calculated from atomistic simulations.

Q_3, in sample A [schematic shown in Fig. 2(a)]. We understand that the one-electron (three-electron) qubit corresponds to an electron occupying the lower (higher) energy valley state v_- (v_+) [15]. We could not achieve three-electron spin resonance for Q_2 as it was strongly coupled to the other dots. In Fig. 2(c) we see that the g_- of Q_1 has an opposite dependence on F_z compared to that of the one QD in sample B. These observed variations in both the Stark shifts and the g-factors qualitatively agree with the theoretically predicted variations shown in Fig. 1. We therefore conclude that these experimentally observed variations are primarily due to different interface conditions associated with each of the QDs.

We also observe variations in the measured T_2^* times, extracted by performing Ramsey experiments [26], for both valley states of the three QDs in sample A, as shown in Fig. 2(d).

The dephasing time due to nuclear spin fluctuations is given in Refs. [28,29], and in our samples, which employ an isotopically enriched ^{28}Si substrate, these times are very long. In the absence of nuclear spin, we can relate T_2^* times with electrical noise in a similar way,

$$T_2^* = \frac{\sqrt{2}\hbar}{\sum_{i=x,y,z} \Delta F_i \left|\frac{dg}{dF_i}\right| \mu_B B_{ext}}. \quad (3)$$

Here, ΔF_i is the standard deviation of the electric field fluctuation seen by the dot, due to electrical noise on the gate. As all of the dots are formed directly underneath the gates, any fluctuation in the top gate (e.g., fluctuation in G_1 for Q_1) will dominate the total field fluctuation. A fluctuation in the top gate will cause $\Delta F_z \gg \Delta F_{x/y}$. From our Sentaurus technology computer-aided design (TCAD) simulations [26], we find that $\frac{\Delta F_z}{\Delta V_g^{top}} = -5.34\ \mu$m^{-1} and $\frac{\Delta F_x}{\Delta V_g^{top}} = 0.2\ \mu$m^{-1}, whereas $\frac{\Delta F_z}{\Delta V_g^{side}} = -3.52\ \mu$m^{-1} and $\frac{\Delta F_x}{\Delta V_g^{side}} = -1.52\ \mu$m^{-1} [26] for a 5-nm gate separation [Fig. 2(a)]. Here, ΔV_g^{top} (ΔV_g^{side}) is a voltage fluctuation in the top (side) gate. A larger gate separation will reduce $\frac{\Delta F_{x/y/z}}{\Delta V_g^{side}}$.

The observed variations in T_2^* can be explained from the changes in $\frac{dg_\pm}{dF_z}$ and $\frac{dg_\pm}{dF_x}$ with interface step location, as shown in Figs. 3(a) and 3(b). When we compare the T_2^* times between the two valley states of Q_1, we see $T_2^*(v_-, Q_1) \approx 1.7\ T_2^*(v_+, Q_1)$, and from Ref. [15] we find $|\frac{dg_+^{Q_1}}{dF_z}| \approx 2.2\ |\frac{dg_-^{Q_1}}{dF_z}|$. This almost linear dependence of $\frac{1}{T_2^*}$ on $|\frac{dg_\pm}{dF_z}|$ shows the dominating contribution of ΔF_z on T_2^* for Q_1. However, comparing Figs. 3(a) and 3(b) we see that $|\frac{dg_\pm}{dF_x}|$ can be larger than $|\frac{dg_\pm}{dF_z}|$ depending

on the interface condition. In the presence of steps and SOI, the up and down spin wave functions move away from each other. For steps parallel to the y direction, $\langle\downarrow|x|\downarrow\rangle \neq \langle\uparrow|x|\uparrow\rangle$, and hence $|\frac{dg_\pm}{dF_x}|$ becomes nonzero. Further details about $\frac{dg_\pm}{dF_{x/y}}$ are presented in the Supplemental Material [26].

The calculations of Figs. 1 and 3 and the experimental observations of Fig. 2 highlight the device-to-device variability issues that would require individual knowledge of each qubit, and impose a challenge to the implementation of a large-scale quantum computer. Any possible way of reducing the variability is crucial to the scale-up of Si QD spin qubits. Also, an increase in T_2^*, regardless of the interface condition, will aid scalability. Next, we investigate ways to improve these issues.

One obvious way to suppress these variabilities is to minimize interface roughness, which is a well-known fabrication challenge. Here, we propose an alternate approach. As predicted in Ref. [18], the g-factors in a Si QD are anisotropic. We can study the anisotropy from a simplified expression [18,26],

$$\delta g_\pm \approx 2\frac{|e|\langle z\rangle}{\mu_B\hbar}(-\alpha_\pm + \beta_\pm \sin 2\phi). \tag{4}$$

Here, ϕ is the angle of B_{ext} with the [100] crystal orientation. From Eq. (4) we see that the contribution of the Dresselhaus SOI is anisotropic and can be tuned by changing the direction of B_{ext}. For example, when B_{ext} is along [100], $\phi = 0^\circ$, and

$$\delta g_\pm^{[100]} \approx -2\frac{|e|\langle z\rangle}{\mu_B\hbar}\alpha_\pm. \tag{5}$$

Comparing Eqs. (2) and (5) we see that $\frac{\delta g_\pm^{[100]}}{\delta g_\pm^{[110]}} \approx \frac{\alpha_\pm}{\beta_\pm}$. As the effect of the monatomic steps is more dramatic on $\beta_\pm$, the change in $g_\pm$ and $\frac{dg_\pm}{dF_z}$ with interface steps should be smaller for B_{ext} along [100] compared to that for [110]. Moreover, since $\beta_\pm \gg \alpha_\pm$ [18,21], $\frac{dg_\pm}{dF_z}$ itself will be much smaller for [100].

Figure 3(a) also compares variations in $\frac{dg_\pm}{dF_z}$ with x_0 between B_{ext} along [110] and [100]. Though there are variations in $\frac{dg_\pm}{dF_z}$ with x_0 for B_{ext} along [100], as shown by the inset of Fig. 3(a), these variations and also $\frac{dg_\pm}{dF_z}$ themselves are negligible, when compared to that along [110]. We see a similar reduction in $\frac{dg_\pm}{dF_x}$ (and its variability with x_0) for B_{ext} along [100] in Fig. 3(b). A variation of $g_\pm$ with x_0 will also be negligible for B_{ext} along [100] [30], as shown in Fig. 3(c). Such phenomena will have a critical impact on the realization of a large-scale quantum computer made of Si QDs. If the external magnetic field is along the [100] crystal orientation, all the qubits will have negligible variations in $g_\pm$, $\frac{dg_\pm}{dF_z}$, $\frac{dg_\pm}{dF_{x/y}}$, and consequently in T_2^* even in the presence of varying interface conditions. Very small $|\frac{dg_\pm}{dF_z}|$ and $|\frac{dg_\pm}{dF_{x/y}}|$ along [100] would also result in very long T_2^* times.

In Fig. 3(d), the angular dependence of $\frac{1}{T_2^*} = \frac{1}{T_2^*(\Delta F_z)} + \frac{1}{T_2^*(\Delta F_x)}$ for $x_0 = -6$ nm, is shown. Here, $T_2^*(\Delta F_{z/x}) = \frac{\sqrt{2}\hbar}{\Delta F_{z/x}|\frac{dg}{dF_{z/x}}|\mu_B B_{\text{ext}}}$. As the monatomic step used in the calculation is parallel to the [010] crystal orientation, $\frac{dg_\pm}{dF_y}$ and thus $T_2^*(\Delta F_y)$ is negligible. A similar angular dependence of $\frac{1}{T_2^*}$ for $x_0 = 0$ nm is shown in the Supplemental Material [26]. We can see here that a large increase in T_2^* (> 1 ms) is achievable by orientating B_{ext} along [100]/[010]/[$\bar{1}$00]/[0$\bar{1}$0].

Now, a decrease in $|\frac{dg_\pm}{dF_z}|$ would also mean a reduced tunability of the g-factors, which is necessary for the selective addressing of individual qubits. However, an increase in T_2^* times will result in a narrower electron spin resonance (ESR) linewidth, $\delta f_{\text{FWHM}} = \frac{2\sqrt{\ln 2}}{\pi T_2^*}$ [9], which would then require a smaller difference in g-factors between qubits to individually address them.

Orienting the magnetic field along the [100] crystal orientation results in a Dresselhaus SOI with only off-diagonal components [26]. Therefore, electric field fluctuations, to first order, contribute to spin dephasing through the weaker Rashba SOI, ensuring a long T_2^* time. At the same time, a resonant oscillating electric field can induce electric dipole spin resonance (EDSR) through the off-diagonal Dresselhaus coupling. Since T_2^* is long under these conditions, coherent operations can be expected even for relatively weak EDSR driving strength, and without invoking the use of micromagnets [9].

To conclude, the presence of random monatomic steps at the interface of a Si QD can cause variations in both the sign and magnitude of the Dresselhaus SOI among neighboring Si QDs. As a result, the electron g-factors and their sensitivity to electric field should vary, which also leads to variability in the dephasing times among quantum dot spin qubits in Si. The extent of these variations is such that g-factors, Stark shifts, and dephasing times for the v_- valley state can be larger than that of the v_+ valley state for some dots while vice versa for others, even with a similar range of vertical electric field across the dots. Likewise, the Stark shifts for the same valley state can change sign between dots. We also experimentally observe such variations, consistent with the theoretical understanding. We further show that even in the presence of interface steps we can control and minimize these variations by taking advantage of the anisotropic nature of SOI in a Si QD. Importantly, we can increase T_2^* times if we align the external magnetic field along the [100] crystal orientation, rather than along [110], which will also help to reduce the SOI-induced dephasing in Si QD devices with integrated micromagnets, as SOI also contributes to the g-factors in these devices [18]. These theoretical findings will guide future experiments to dig into the variability issues in detail and explore the role of the spin-orbit interaction in Si QDs.

This work was supported by the U.S. Army Research Office (W911NF-13-1-0024, W911NF-12-0607), the Australian Research Council (CE11E0001017), and the NSW Node of Australian National Fabrication Facility. Computational resources on nanoHUB.org, funded by NSF Grant No. EEC-0228390, were used.

[1] L. M. K. Vandersypen, H. Bluhm, J. S. Clarke, A. S. Dzurak, R. Ishihara, A. Morello, D. J. Reilly, L. R. Schreiber, and M. Veldhorst, npj Quantum Inf. **3**, 34 (2017).

[2] D. Loss and D. P. DiVincenzo, Phys. Rev. A **57**, 120 (1998).

[3] F. A. Zwanenburg, A. S. Dzurak, A. Morello, M. Y. Simmons, L. C. L. Hollenberg, G. Klimeck, S. Rogge, S. N. Coppersmith, and M. A. Eriksson, Rev. Mod. Phys. **85**, 961 (2013).

[4] K. M. Itoh and H. Watanabe, MRS Commun. **4**, 143 (2014).

[5] B. M. Maune, M. G. Borselli, B. Huang, T. D. Ladd, P. W. Deelman, K. S. Holabird, A. A. Kiselev, I. Alvarado-Rodriguez, R. S. Ross, A. E. Schmitz, M. Sokolich, C. A. Watson, M. F. Gyure, and A. T. Hunter, Nature (London) **481**, 344 (2012).

[6] D. Kim, Z. Shi, C. B. Simmons, D. R. Ward, J. R. Prance, T. S. Koh, J. K. Gamble, D. E. Savage, M. G. Lagally, M. Friesen, S. N. Coppersmith, and M. A. Eriksson, Nature (London) **511**, 70 (2014).

[7] X. Wu, D. R. Ward, J. R. Prance, D. Kim, J. K. Gamble, R. T. Mohr, Z. Shi, D. E. Savage, M. G. Lagally, M. Friesen, S. N. Coppersmith, and M. A. Eriksson, Proc. Natl. Acad. Sci. USA **111**, 11938 (2014).

[8] M. Veldhorst, J. C. C. Hwang, C. H. Yang, A. W. Leenstra, B. de Ronde, J. P. Dehollain, J. T. Muhonen, F. E. Hudson, K. M. Itoh, A. Morello, and A. S. Dzurak, Nat. Nanotechnol. **9**, 981 (2014).

[9] E. Kawakami, P. Scarlino, D. R. Ward, F. R. Braakman, D. E. Savage, M. G. Lagally, M. Friesen, S. N. Coppersmith, M. A. Eriksson, and L. M. K. Vandersypen, Nat. Nanotechnol. **9**, 666 (2014).

[10] K. Eng, T. D. Ladd, A. Smith, M. G. Borselli, A. A. Kiselev, B. H. Fong, K. S. Holabird, T. M. Hazard, B. Huang, P. W. Deelman, I. Milosavljevic, A. E. Schmitz, R. S. Ross, M. F. Gyure, and A. T. Hunter, Sci. Adv. **1**, e1500214 (2015).

[11] M. Veldhorst, C. H. Yang, J. C. C. Hwang, W. Huang, J. P. Dehollain, J. T. Muhonen, S. Simmons, A. Laucht, F. E. Hudson, K. M. Itoh, A. Morello, and A. S. Dzurak, Nature (London) **526**, 410 (2015).

[12] D. M. Zajac, T. M. Hazard, X. Mi, E. Nielsen, and J. R. Petta, Phys. Rev. Appl. **6**, 054013 (2016).

[13] C. Jones, M. A. Fogarty, A. Morello, M. F. Gyure, A. S. Dzurak, and T. D. Ladd, arXiv:1608.06335.

[14] M. Veldhorst, H. G. J. Eenink, C. H. Yang, and A. S. Dzurak, Nat. Commun. **8**, 1766 (2017).

[15] M. Veldhorst, R. Ruskov, C. H. Yang, J. C. C. Hwang, F. E. Hudson, M. E. Flatté, C. Tahan, K. M. Itoh, A. Morello, and A. S. Dzurak, Phys. Rev. B **92**, 201401(R) (2015).

[16] P. Scarlino, E. Kawakami, D. R. Ward, D. E. Savage, M. G. Lagally, M. Friesen, S. N. Coppersmith, M. A. Eriksson, and L. M. K. Vandersypen, Phys. Rev. Lett. **115**, 106802 (2015).

[17] P. Scarlino, E. Kawakami, T. Jullien, D. R. Ward, D. E. Savage, M. G. Lagally, M. Friesen, S. N. Coppersmith, M. A. Eriksson, and L. M. K. Vandersypen, Phys. Rev. B **95**, 165429 (2017).

[18] R. Ferdous, E. Kawakami, P. Scarlino, M. P. Nowak, D. R. Ward, D. E. Savage, M. G. Lagally, S. N. Coppersmith, M. Friesen, M. A. Eriksson, L. M. K. Vandersypen, and R. Rahman, arXiv:1702.06210.

[19] L. E. Golub and E. L. Ivchenko, Phys. Rev. B **69**, 115333 (2004).

[20] M. O. Nestoklon, L. E. Golub, and E. L. Ivchenko, Phys. Rev. B **73**, 235334 (2006).

[21] M. O. Nestoklon, E. L. Ivchenko, J.-M. Jancu, and P. Voisin, Phys. Rev. B **77**, 155328 (2008).

[22] C. H. Yang, A. Rossi, R. Ruskov, N. S. Lai, F. A. Mohiyaddin, S. Lee, C. Tahan, G. Klimeck, A. Morello, and A. S. Dzurak, Nat. Commun. **4**, 2069 (2013).

[23] H. J. W. Zandvliet and H. B. Elswijk, Phys. Rev. B **48**, 14269 (1993).

[24] M. Friesen, M. A. Eriksson, and S. N. Coppersmith, Appl. Phys. Lett. **89**, 202106 (2006).

[25] N. Kharche, M. Prada, T. B. Boykin, and G. Klimeck, Appl. Phys. Lett. **90**, 092109 (2007).

[26] See Supplemental Material at http://link.aps.org/supplemental/10.1103/PhysRevB.97.241401 for details about the analytic model, Ramsey experiments, effects of the in-plane electric field on the g-factors, and Sentaurus TCAD simulations.

[27] L. M. Roth, Phys. Rev. **118**, 1534 (1960).

[28] R. Hanson, L. P. Kouwenhoven, J. R. Petta, S. Tarucha, and L. M. K. Vandersypen, Rev. Mod. Phys. **79**, 1217 (2007).

[29] I. A. Merkulov, Al. L. Efros, and M. Rosen, Phys. Rev. B **65**, 205309 (2002).

[30] Recently, we became aware of an experimental work [R. M. Jock *et al.*, Nat. Commun. **4**, 1768 (2018)] that measures the difference in g-factors between two neighboring QDs in a Si/SiO_2 sample for different directions of B_{ext}. Their findings validate our prediction. The authors also observe a further reduction in the g-factor difference for B_{ext} along the [001] direction, due to the suppression of both the Rashba and Dresselhaus SOI along [001], while for [100] only the Dresselhaus SOI gets suppressed. However, we need at least some tunability of the g-factor ($\frac{dg}{dF_z}$) to selectively address the qubits, which is possible through the weaker Rashba SOI along [100] but might not be possible along [001].